Accurate equivalent-circuit descriptions of thin glide-symmetric corrugated metasurfaces,

Guido Valerio, Zvonimir Sipus, Anthony Grbic, Oscar Quevedo-Teruel

Accurate Equivalent-Circuit Descriptions of Thin Glide-Symmetric Corrugated Metasurfaces

Guido Valerio, Zvonimir Sipus,
Anthony Grbic, and Oscar Quevedo-Teruel

***Abstract*—Thin artificial surfaces that act as high frequency band-gap structures have been recently studied for the design of gap waveguides, hard surfaces, and planar lenses. Here, we propose a circuit-based method to analyse glide-symmetric corrugated metasurfaces that are embedded in a thin parallel plate waveguide. Our closed-form solution is based on rigorous analytical derivations. It achieves remarkable agreement with full-wave solvers, even when the waveguide thickness is extremely thin. In contrast, classical homogenization approaches are shown to be inaccurate for thin waveguides due to the interaction of higher-order Floquet modes between the surfaces. Numerical results validate our theoretical analysis and show the utility of the proposed method.**

***Index Terms*—Equivalent circuit, homogenization, transverse resonance method, dispersive analysis, corrugated surfaces, metasurfaces, planar lenses, glide symmetry.**

I. Introduction

Metasurfaces have emerged as an attractive solution for next generations planar devices that control wave propagation at millimeter waves [1]. Their low-cost, light-weight and simple integration with electronic circuits make them an interesting candidate for reduced-losses guiding-wave and high-gain radiating devices [2]-[5]. In addition, artificial gradient-index metasurfaces have been employed to create beam scanning planar lens antennas [6], [7], [8], avoiding the use of conventional lossy, expensive and bulky beam-forming networks [9]. A number of artificial lenses embedded in parallel-plate-waveguide (PPW) technology have also been proposed [10]-[12].

Although these initial works are very promising, there have been obstacles to the adoption of this technology as a competitive alternative to well-established techniques. For example, initial implementations had a narrow bandwidth of operation, due to their strong frequency dispersion. This led to significant variations of the effective refractive index with frequency. Furthermore, planar PPW metasurface lenses usually require the presence of a dielectric slab [7]. The dielectric slab may produce high losses arising from the presence of high current densities on the small printed metallizations. Finally, the dielectric slab must be truncated at the lens aperture to produce radiation. However, the presence of waves mainly confined in the dielectric inherently produces a mismatch between the lens and the free-space region.

It has been recently demonstrated in [13] that these disadvantages can be overcome by using all-metallic metasurfaces in a PPW. In order to increase the bandwidth of operation and the equivalent refractive index range, glide symmetry may be employed. Glide symmetry means that *both* the upper and the lower PPW plates possess a periodic texture that are shifted by a half period with respect to each other [14].

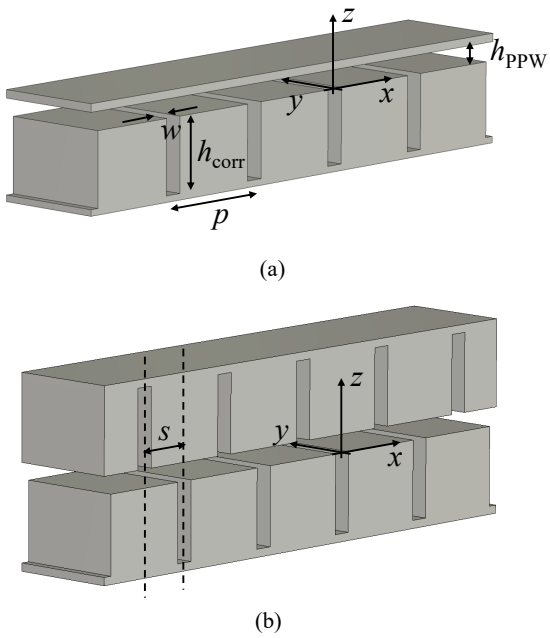

Figure 1. Geometry of the structures investigated in this paper, with definition of the relevant geometric parameters. The origin of the axes is taken on the lower PPW plate, in the middle of a groove (i.e., the unit-cell groove of the lower plate lies on the plane $z = 0$ for $|x| < w/2$.). The upper PPW plate is at $z = h_{\mathrm{PPW}}$. (a) PPW with a bottom corrugated plate. (b) PPW with two corrugated plates, whose corrugations are shifted one respect to the other of an arbitrary length, s. If $s = p/2$, the structure is glide-symmetric.

Since the interesting properties of glide symmetry structures have only been recently discovered [13],[15], specific analysis methods have not yet been proposed. In fact, modeling of these types of structures imposes fundamental limitations due to the presence of geometrical details at different scales: *thin PPW slabs* and relatively *large inclusions* (corrugations, pins or holes). This contrast in scales is required to obtain UWB performance in 2D-lenses [13] and is a requirement in gap waveguide technology [3],[15]. These fundamental limitations are due to the close spacing of the textured plates, leading to the interaction of high-order Floquet modes and a complex field distribution on the metasurfaces. As a consequence, conventional homogenized formulas for periodic surfaces [16] have a reduced accuracy. On the other hand, full-wave models become prohibitively time-consuming if a large structure must be simulated [17].

In this paper, we propose different methods to study the dispersion diagram of corrugated structures, including glide-symmetric metasurfaces. For simplicity, two-dimensional structures periodic in one dimension are studied. These structures are uniform along one horizontal direction and periodic along the other. The vertical direction is the direction orthogonal to the PPW plates (see Fig. 1). To begin, a single-layer of corrugations in a thin PPW is considered (see Fig. 1(a)). Since the PPW is thin, we propose a high-order surface admittance method to accurately model the metasurface. Then, arbitrary field variations on each corrugation and Floquet modes are taken into account. However, this version of the method cannot be used for glide-symmetric structures (see Fig. 1(b)). Therefore, a second model, valid also for glide-symmetric structures is introduced here. In this second method, the corrugations are described with an equivalent two-port network, considering a transmission line along

Manuscript received Month XX, 2016; revised Month XX, 2016.

This work was supported in part by the Spanish Government under Project TEC2013-44019-R, and by the Swedish STINT Postdoctoral Transition Grants programme under Grant PT2014-5813 funded by the Swedish Foundation for International Cooperation in Research and Higher Education.

G. Valerio is with Sorbonne Universités, UPMC Univ. Paris 06, UR2, L2E, F-75005 Paris, France. e-mail: (guido.valerio@upmc.fr).

Z. Sipus is with with the Faculty of Electrical Engineering and Computing, University of Zagreb, Unska 3/XII, HR-10000 Zagreb, Croatia. e-mail: (zvonimir.sipus@fer.hr).

A. Grbic is with the Radiation Laboratory at the Department of Electrical Engineering and Computer Science, University of Michigan, Ann Arbor, MI, 48109-2122 USA. e-mail: (agrbic@umich.edu).

O. Quevedo-Teruel is with with the Department of Electromagnetic Engineering, School of Electrical Engineering, KTH Royal Institute of Technology, SE-100 44, Sweden. e-mail: (oscarqt@kth.se).

the propagation direction [18], [19].

The paper is organized as follows. In Section II, the standard homogenized admittance for corrugated surfaces is briefly reviewed. In Section III, a derivation of the homogenized high-order surface admittance is described. In Section IV, the equivalent longitudinal-circuit network is described, and in Section V, the implementation of the method for glide-symmetric structures is discussed. In Section VI, numerical results from the two methods are compared with those of a commercial solver to validate the accuracy of the proposed methods. In Section VII, conclusions are drawn.

II. Unimodal Homogenized-Admittance Approach

A single-corrugated waveguide, as shown in Fig. 1(a), has been extensively studied by replacing the corrugated surface with an homogenized admittance [16]. However, this approach is not possible for the case of glide-symmetric structures, as shown in Fig. 1(b). A single-corrugated waveguide consists of a PPW in which one of the metallic plates is replaced with a corrugated surface. The period of corrugations is denoted with p, the width of the groove with w, their depth with h_{corr}, and the PPW height with h_{PPW}. A time harmonic dependence of $e^{j\omega t}$ is assumed throughout this paper. The structure is two-dimensional, i.e. invariant along the y direction. Additionally, we consider a TM^x mode propagation along the horizontal x direction, having field components E_x, E_z, H_y.

If the fields are assumed to be constant along the corrugations, and the PPW thickness h_{PPW} is sufficiently large to disregard vertical interactions through higher-order attenuated Floquet modes, the corrugated surface can be replaced with an impedance surface. This admittance Y is obtained by computing the ratio between the magnetic and electric field tangential to the surface $H_y^{\mathrm{corr}}/E_x^{\mathrm{corr}}$ [20]:

$$Y = \frac{H_y^{\mathrm{corr}}\left(x, z=0\right)}{E_x^{\mathrm{corr}}\left(x, z=0\right)} = \frac{j}{\eta_0}\frac{p}{w}\cot\left(k_0 h_{\mathrm{corr}}\right) \tag{1}$$

The accuracy of the approach can be increased by accounting for higher-order harmonic interaction and field singularities at the edge of the grooves. With these assumptions, a modified equivalent admittance is obtained in [21] yielding perfect agreement with full-wave simulations of a single corrugated surface. Although this kind of approaches is usually very accurate, the presence of the upper plate at a short distance from the corrugated surface will cause the need to include not only higher-order harmonics in the PPW, but also a horizontal variation of the field along the groove. This variation depends on frequency, and becomes especially relevant when the ratio w/p approaches to unity (i.e., large corrugations). The inaccuracy of (1) in these particular cases will be discussed in Section VI.

III. Multimodal Admittance Approach

In this section, we include higher-order Floquet modes in order to overcome the limitations in accuracy of the unimodal admittance model for a single-corrugated waveguide, Fig. 1(a). Additionally, a more complex field variation on the groove width is employed. Relating electric and magnetic fields on the corrugations, a multimodal admittance will be obtained.

Specifically, the field representation inside the corrugations is

$$H_y^{\mathrm{corr}}\left(x,z\right) = \sum_{n=0}^{N} \alpha_n \tilde{H}_{y,n}\left(x,z\right), \tag{2}$$

$$E_x^{\mathrm{corr}}\left(x,z\right) = \sum_{n=0}^{N} \alpha_n \tilde{E}_{x,n}\left(x,z\right) \tag{3}$$

with

$$\tilde{H}_{y,n} = \cos\left[\frac{n\pi}{w}\left(x+\frac{w}{2}\right)\right]\cos\left[k_{z,n}\left(z+h_{\mathrm{corr}}\right)\right] \tag{4}$$

and

$$\tilde{E}_{x,n} = -\frac{j\eta_0 k_{z,n}}{k_0}\cos\left[\frac{n\pi}{w}\left(x+\frac{w}{2}\right)\right]\sin\left[k_{z,n}(z+h_{\mathrm{corr}})\right] \tag{5}$$

where $k_{z,n} = \sqrt{k_0^2 - \left(\frac{n\pi}{w}\right)^2}$ is the vertical wavenumber of the nth mode of the waveguide. One can determine the higher-order surface admittance terms $\tilde{Y}_n$ as

$$\tilde{Y}_n = \frac{\tilde{H}_{y,n}}{\tilde{E}_{x,n}} = \frac{jk_0}{\eta_0 k_{z,n}}\frac{p}{w}\cot\left(k_{z,n}h_{\mathrm{corr}}\right) \tag{6}$$

A diagonal admittance matrix $\underline{\mathbf{Y}}$ can be defined, whose (n,n) element is $\tilde{Y}_n$. This definition generalizes the unimodal admittance in (1). As in that case, it leads to an expression for the magnetic field on the surface $z=0$, which is proportional to the electric field on the same surface:

$$\mathbf{h}_y = \underline{\mathbf{Y}}\cdot\mathbf{e}_x^T \tag{7}$$

where T stands for a vector transposition, and

$$\mathbf{h}_y = \left(\tilde{H}_{y,1}, \tilde{H}_{y,2}, \ldots, \tilde{H}_{y,N}\right)\Big|_{z=0} \tag{8}$$

$$\mathbf{e}_x = \left(\tilde{E}_{x,1}, \tilde{E}_{x,2}, , \ldots, \tilde{E}_{x,N}\right)\Big|_{z=0}. \tag{9}$$

In order to determine α_n in (2) and (3), expressions for fields in the PPW region are needed to express boundary conditions on the corrugation. Due the periodicity in the x direction within the PPW, the field can be represented with the following double summation:

$$H_y^{\mathrm{PPW}} = \sum_{n=0}^{N}\alpha_n \sum_{i=-\mathrm{NF}}^{\mathrm{NF}} \xi_{n,i}\cos\left[k_{z,i}(z-h_{\mathrm{PPW}})\right]e^{-jk_{x,i}x} \tag{10}$$

$$\begin{aligned} E_x^{\mathrm{PPW}} = -\frac{j\eta_0}{k_0}\sum_{n=0}^{N}\alpha_n \sum_{i=-\mathrm{NF}}^{\mathrm{NF}} \xi_{n,i}k_{z,i} \\ \times \sin\left[k_{z,i}(z-h_{\mathrm{PPW}})\right]e^{-jk_{x,i}x} \end{aligned} \tag{11}$$

with $k_{x,i} = k_x + 2\pi i/p$, and $2\mathrm{NF}+1$ is the number of Floquet modes retained in the summation. From the E-field boundary condition on the corrugated surfaces and as a consequence of orthogonality of propagating Floquet modes, the coefficients $\xi_{n,i}$ are determined by

$$\begin{aligned} \xi_{n,i} = -\frac{k_{z,n}\sin\left(k_{z,n}h_{\mathrm{corr}}\right)}{k_{z,i}\sin\left(k_{z,i}h_{\mathrm{PPW}}\right)} \\ \times \frac{1}{p}\int_{-w/2}^{w/2}\cos\left[\frac{n\pi}{w}\left(x+\frac{w}{2}\right)\right]e^{+jk_{x,i}x}\mathrm{d}x. \end{aligned} \tag{12}$$

The relative amplitude of each corrugation mode α_n is determined by applying the mode-matching procedure, i.e. after testing the continuity equation for the tangential component of the magnetic field with suitable test functions. A Galerkin approach is chosen here, i.e., the (mutually orthogonal) testing functions are:

$$f_m(x) = \cos\left[\frac{m\pi}{w}\left(x+\frac{w}{2}\right)\right], \qquad m = 0, 1, \ldots, N. \tag{13}$$

In the absence of a source, the resulting set of linear equations is homogeneous. Zeros of the linear-system determinant are k_x values of the Floquet modes of the corrugated waveguide.

IV. Longitudinal-Circuit Approach

The homogenized admittance used in Section II is an attractive description of the corrugated PPW: it replaces a periodic structure with a homogeneous one. By establishing a *transverse* transmission line along the z axis, the dispersion diagram can be easily obtained since the surface impedance is known in closed form. Unfortunately, its accuracy rapidly deteriorates when the PPW are very thin. The method used in Section III overcomes this limitation, but requires

the numerical determination of the field on the corrugation apertures through a Galerkin testing procedure, and thus cannot give the relevant dispersion diagram in closed form.

In this section, we propose a different circuit approach by establishing this time a *longitudinal* transmission line along the periodicity x direction instead of the transverse z direction. Knowledge of the circuit parameters of a unit cell lead to a straightforward evaluation of the wavenumber of Bloch modes by considering a cascade of unit cells in a periodic configuration [22],[23]. It should be stressed that the present approach can be generalized to a two-dimensional lattice [24].

The unit cell considered here is known in microwave waveguide theory as a "T-junction," consisting of a junction between orthogonal parallel waveguides, as shown in Fig. 2(b). In our structure, one of the two waveguides composing the T-junction is shorted with a metallic plane at its end (top side). The length of the shorted waveguide corresponds to the depth of the corrugation $h_{\rm corr}$. The height of this PPW (w) may be thick, in contrast to the other, whose height is $h_{\rm PPW}$ (possibly very small).

The T-junction has been extensively studied in the framework of waveguide-based guiding and leaky-wave devices, and accurate circuit models have been proposed [18], [25]. These models are based on mode matching: imposing field continuity on the planes defining the junction. The fields are computed by retaining two PPW vertical modes. In this way, interactions between the corrugated surface and the upper plate are taken into account in the circuit model, and reliable results can be obtained even in the case of thin structures, as it will be demonstrated in Section VI.

From the different circuits proposed, the one by Marcuvitz [18] is selected here to study the corrugated PPW. Its range of validity is within 10% as long as both PPW thickness and groove width are smaller than half a wavelength ($h_{\rm PPW} < \lambda/2$ and $w < \lambda/2$). A more accurate circuit has been proposed in [25] for values of $h_{\rm PPW}$ close to $\lambda/2$. However, these validity limits are never reached in our applications. In low-profile surfaces, the PPW height is always smaller than 0.1λ. Furthermore, the groove width is always smaller than the unit-cell length, hence in subwavelength cells the groove is always much smaller than the wavelength. This will be confirmed by the numerical results shown in Section VI. An alternative circuit for corrugated surfaces is proposed in [21], where different higher-order harmonics and different modes in the corrugations can be retained, thus tuning the required accuracy. However, a uniform electric field on the groove aperture (apart from edge singularities) is there considered. Since the mode-matching formulation of Sec. III confirms a non-negligible impact of field variation along each aperture, Marcuvitz's circuit is employed here.

In order to summarize the results, the relevant formulas for the circuit parameters of the unit cell in Fig. 2(b) are given below ((14)-(21)):

$$B_{\rm sh} = \frac{1}{\eta_0}\cot\left(k_0 l\right) \tag{14}$$

$$B_a = \frac{2w}{\lambda_0\eta_0}\left(\arctan\frac{1}{\alpha} + \frac{\ln\sqrt{1+\alpha^2}}{\alpha}\right) \tag{15}$$

$$B_c = \frac{\lambda_0}{2\pi w\eta_0} \tag{16}$$

$$B_a - 2B_b = \frac{2h_{\rm PPW}}{\lambda_0\eta_0}\left(\frac{\pi}{3\alpha} + A_1\right) \tag{17}$$

$$B_d = \frac{w}{\lambda_0\eta_0}\left(\frac{\pi}{3\alpha} + A_2\right) \tag{18}$$

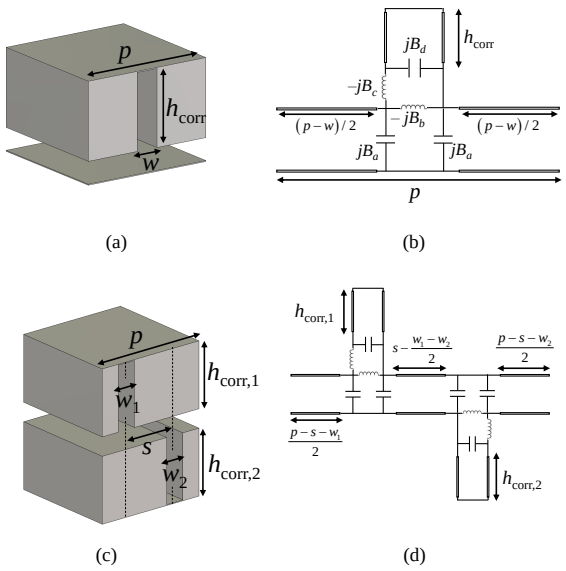

Figure 2. Geometry of unit cell used in the structures in Fig. 1. (a) Unit cell for the single-corrugated PPW in Fig. 1(a). (b) Circuit model of the unit cell of the single-corrugated cell. (c) Unit cell for the double-corrugated PPW in Fig. 1(b) (d) Circuit model of the unit cell of the double-corrugated cell. If $w_1 = w_2$, $h_{\rm corr,1} = h_{\rm corr,2}$ and $s = p/2$ the cell is glide-symmetric.

where, $2\alpha = h_{\rm PPW}/w$, $\eta_0 = 120\pi$ is the free-space impedance, and

$$A_1 = -\frac{2\alpha}{\pi}e^{-\frac{2\arctan\alpha}{\alpha}}\left\{1 + \frac{5+\alpha^2}{4\left(1+\alpha^2\right)}e^{-\frac{2\arctan\alpha}{\alpha}} + \right. \tag{19}$$

$$\left. + \frac{4}{1+\alpha^2} + \left(\frac{5+\alpha^2}{1+\alpha^2}\right)^2\frac{e^{-\frac{4\arctan\alpha}{\alpha}}}{9}\right\} \tag{20}$$

$$\frac{A_1 + A_2}{2} =$$

$$\alpha\arctan\frac{1}{\alpha} + \frac{\arctan\alpha}{\alpha} + \ln\frac{1+\alpha^2}{4\alpha} - \frac{\pi\left(1+\alpha^2\right)}{6\alpha} \tag{21}$$

The expressions are obtained by applying Marcuvitz's circuits for a short-circuit junction. The corrugation is equivalent to a short-circuit series stub. The higher-order interaction, which plays a relevant role for thin structures and large corrugation widths, are described by the reactive elements placed at the junction planes. Once the unit-cell parameters are obtained, a periodic cascade of cells can be considered in order to perform dispersion analysis. The wavenumber of the fundamental Bloch-mode supported by the periodic structure can be expressed in terms of its $ABCD$ matrix as [22],[23]:

$$\cos\left(k_x p\right) = \frac{A\left(f\right) + D\left(f\right)}{2} = A\left(f\right) \tag{22}$$

$A\left(f\right)$ and $D\left(f\right)$ are the first and fourth elements of the unit cell's $ABCD$ matrix, written explicitly as a function of the frequency f. It is assumed that $A\left(f\right) = D\left(f\right)$, since the cell is symmetric.

The equivalent circuit also allows one to derive a simple expression for the frequency $f_{\rm sb}$ of the lower stop-band edge, by imposing the condition $k_x = \pi/p$ at the frequency $f_{\rm sb}$ in (22):

$$A\left(f_{\rm sb}\right) + 1 = 0 \tag{23}$$

A numerical solution of this equation yields a very accurate estimate of the pass-band of the periodic surface. It will be demonstrated in Section VI that refinement through full-wave simulation is not required. Surface design can then be simply performed by tuning the stop-band edge obtained using (23) with a suitable variation of

geometrical parameters (e.g., the depth of the corrugations $h_{\rm corr}$ or the spatial period p).

V. Glide-Symmetric Corrugated Waveguide

Another advantage of the formulation in Section IV is its ability to analytically model a double-corrugated PPW (Fig. 1(b)), whose upper and lower plates are both corrugated and shifted by a distance s. The unit cell of the structure is composed of two corrugations, one on the upper and one on the lower plate, as shown in Fig. 2(c). In other words, the unit cell consists of two T-junctions connected through a simple transmission-line section. In the first junction, the shorted series stub, together with its reactive elements, are placed on the upper line. In the case of the second junction, the same impedances are placed on the lower line, as shown in Fig. 2(d). In order for this model to be valid, we require that the two corrugations do not overlap, i.e., $\min\{s, p-s\} > (w_1+w_2)/2$. As it will be shown in Section VI, perfect agreement with full-wave results is obtained even in the limiting case of $\min\{s, p-s\} = (w_1+w_2)/2$.

Let us consider a glide-symmetric PPW, where $w_1 = w_2 = w$, $h_{\rm corr,1} = h_{\rm corr,2} = h_{\rm corr}$ and $s = p/2$. The structure is invariant under glide symmetry: it is the composition of two geometrical transformations, namely a translation in the x direction of $s = p/2$ and a reflection with respect to the plane $z = h_{\rm PPW}/2$ [14]. Glide-symmetric structures are periodic, but the *minimal* transformation defining them is the glide symmetry. As a consequence, it was shown in [14] that no band-gap occurs at $k_x = \pi/p$. Therefore, the strong frequency dispersion that occurs next to a stop-band edge is not present. As a result, reduced frequency dispersion is obtained over a large range of frequency for modes having high equivalent refractive indexes. This phenomenon was recently reported in one-dimensional structures [26], [27], and extended to 2D-periodic configurations in [13]. These atttractive features could have broad applications in metamaterial design and synthesis.

It is interesting to stress that the stop-band suppression achieved at $k_x = \pi/p$ leads to different features with respect to previous extensive studies focusing on the suppression of open stop-band at $k_x = 0$ for optimized broadside radiation of leaky-wave antennas [28], [29]. However, both phenomena can be regarded as due to specific resonances of the equivalent circuits describing the unit cell of the periodic structure [30], [29].

VI. Numerical Results

In this section, dispersion analysis is performed for PPWs with one or two corrugated plates using the methods described in the previous sections: unimodal homogenized admittance, multi-modal admittance and longitudinal equivalent circuit. These methods are also compared to full-wave results obtained with *CST Microwave Studio* [31]. The real part β of the wavenumber of the fundamental mode k_x of the corrugated PPW will only be considered. This mode is of interest for the design of artificial lenses and gap waveguides.

A. Single-corrugated waveguide

In Fig. 3, the Brillouin diagram of a PPW with a PEC and a corrugated surface (see Fig. 1(a)) is shown for structures having different PPW thicknesses, $h_{\rm PPW}$. In Figs. 3(a),(b), a thick PPW is considered, $h_{\rm PPW} = 3.5$ mm. For a small period, $p = 2$ mm in Fig. 3(a), all the approaches accurately model the structure, independently of the groove width w. In Fig. 3(b), a larger period is considered. In this example, the results obtained using the homogeneous unimodal admittance becomes less accurate. On the other hand, the multimodal admittance and the equivalent longitudinal circuit lead to very accurate results, indistinguishable from CST.

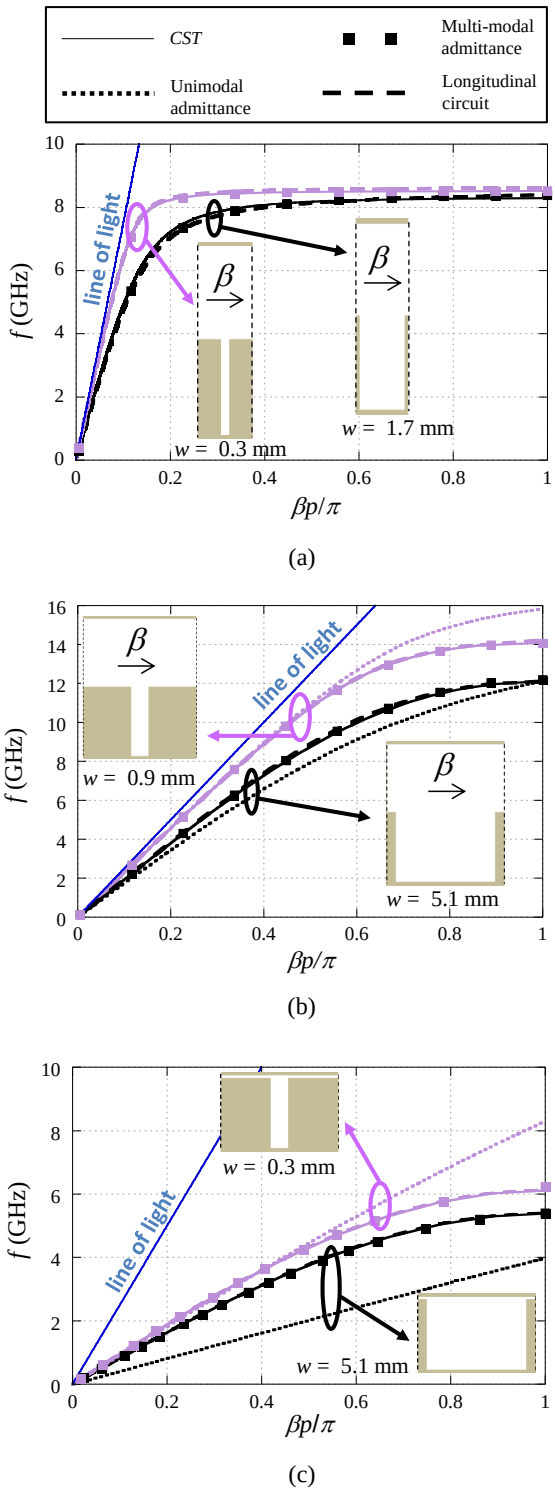

Figure 3. Dispersion diagram for the fundamental mode of a single-corrugated PPW as in Fig. 1(a) for: CST simulations, transverse resonance with the unimodal admittance as in Section II, multimodal admittance as in Section III, longitudinal circuit as in Section IV. $h_{\rm corr} = 4.33$ mm for all cases. (a) $p = 2$ mm and $h_{\rm PPW} = 3.5$ mm (b) $p = 6$ mm and $h_{\rm PPW} = 3.5$ mm (c) $p = 6$ mm and $h_{\rm PPW} = 0.1$ mm.

Finally, in Fig. 3(c), an extremely thin PPW is considered, as in the lens designed in [13] ($h_{\rm PPW} = 0.1$ mm). This design achieves a large variation of the equivalent refractive index together with a UWB frequency response. In this case, due to the strong interactions

between the plates, the simple homogeneous unimodal admittance does not provide accurate results. As anticipated in Section II, the loss of accuracy is particularly significant as the ratio w/p increases. Difficulty in the modeling is also found when using the multimodal admittance: in order to obtain good results, 16 modes in the groove have been retained.

A quantitative division between the thick and the thin case is difficult to find, as the interaction between surfaces increases continuously. In the parameter ranges of interest in our applications (relatively large subwavelength groove width and the absence of a dielectric in the corrugations), a visible discrepancy between results obtained with unimodal and a multimodal admittances arises when $10h_{\mathrm{PPW}} < w$, which corresponds to a relative error of 10%.

These results show that the longitudinal equivalent circuit discussed in Section IV is always able to reproduce the full-wave results, even for the cases when the unimodal admittance fails. Finally, the multimodal homogeneous admittance discussed in Section III can accurately describe the dispersion behavior of the structure, but several modes must be retained in each groove for larger values of w/p combined with an extremely thin PPW.

B. Glide-symmetric corrugations

In Figs. 4(a) and (b), we apply the equivalent longitudinal circuit to the study of glide-symmetric structures, i.e. the corrugations are mutually shifted along the axis of periodicity. In such a configuration, the homogenized admittance method cannot be employed, since after the homogenization procedure, information about the exact location of the corrugation is lost and the shift between the plates cannot be described. Such a shift should be taken into account before the homogenization and leads to a different transverse-resonance condition. Therefore, this approach is not investigated here, and the results of the longitudinal circuit are only compared to those from a the full-wave commercial solver.

Two different PPW thicknesses are considered, as was done for the previous single-corrugated case. The shift between the plates is chosen to be $s = p/2$ leading to a UWB behavior as described in [13]. In Fig. 4(a), the dispersion diagram is shown for a structure whose thickness is $h_{\mathrm{PPW}} = 3.5$ mm, and for two different values of the groove width, a small one ($w = 1$ mm) and a large one ($w = 3$ mm). The latter case is the maximum width which can be handled by our equivalent circuit. If $w > p/2$, a T junction can no longer be defined, due to superposition of the corrugations on the different plates. In Fig. 4(b), the dispersion diagram is shown for a structure whose thickness is $h_{\mathrm{PPW}} = 0.1$ mm, for the same values of the groove width. In order to show the validity of the circuit method, a larger frequency band is included in the figures. Again, the results of the equivalent longitudinal circuit are practically indistinguishable from the full-wave results in this extended frequency range, including higher order modes, even for the extreme case $w = p/2$, both for thick and for extremely thin PPWs. Very small errors start to be visible for higher frequency bands in the thicker PPW, at around 14 GHz, confirming the validity range of the circuit for small values of h_{PPW}/λ. However, the agreement with full-wave results is still reasonably good and sufficient for the most of practical applications.

As noted in Section IV, the equivalent longitudinal circuit is useful for accurately estimating the lower stop-band edge, f_{sb}, by solving (23). In Fig. 5, the left-hand side of (23) is plotted as a function of frequency for several structures differing by their geometrical parameters. The zero of each curve is easily detectable with simple root-searching algorithms, thanks to the smoothness of the curves and to the absence of singularities and asymptotes. It should be emphasized that the curves plotted are known in closed-form and do not arise from any numerical approximation.

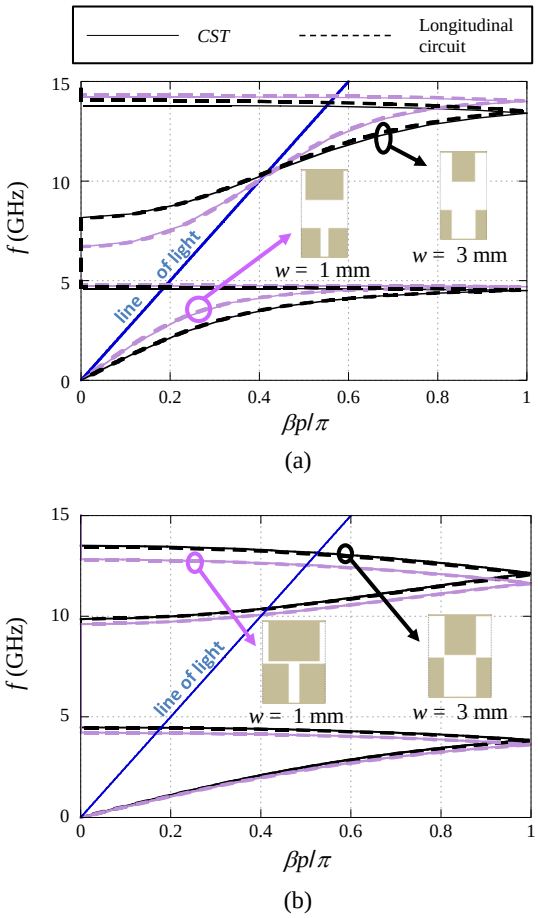

Figure 4. Dispersion diagram of a glide-symmetric PPW as in Fig. 1(b). Comparison between: *CST* simulations, longitudinal circuit as in Section IV. For all the cases: $p = 6$ mm, $h_{\mathrm{corr}} = 15$ mm. (a) $h_{\mathrm{PPW}} = 3.5$ mm. (b) $h_{\mathrm{PPW}} = 0.1$ mm.

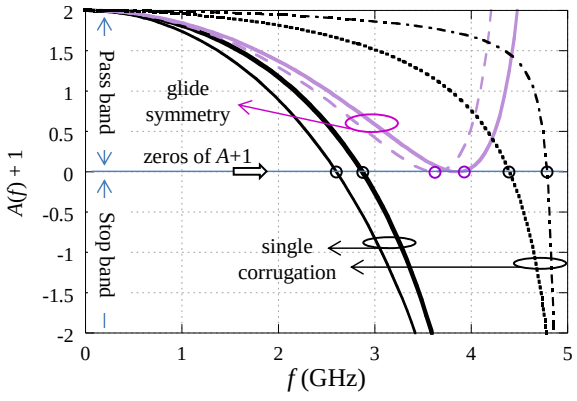

Figure 5. Right-hand side of (23). The zero of each curves corresponds to the lower stop-band edge frequency. For all the cases: $h_{\mathrm{corr}} = 3.44$ mm. Single-corrugated PPW (*black lines*): $w = 5$ mm, $h_{\mathrm{PPW}} = 2$ mm (*dotted line*), $w = 0.5$ mm, $h_{\mathrm{PPW}} = 2$ mm (*dashed-dotted line*), $w = 5$ mm, $h_{\mathrm{PPW}} = 0.1$ mm (*solid thin line*), $w = 1$ mm, $h_{\mathrm{PPW}} = 0.1$ mm (*solid thick line*). Glide symmetry PPW (*violet lines*), with $s = p/2$: $w = 3$ mm, $h_{\mathrm{PPW}} = 0.1$ mm (*solid line*), $w = 1$ mm, $h_{\mathrm{PPW}} = 0.1$ mm (*dashed line*).

It is interesting to note that different propagation regimes are recognizable in this picture with and without the presence of glide symmetry. When the single-corrugated waveguide has values between $-1 < A < 1$ ($0 < A + 1 > 2$ of in the picture), propagating modes with real $k_x = \beta$ exist. These values occur from zero frequency up to the stop-band edge frequency. At higher frequencies, $A < -1$ ($A+1 < 0$ in the picture), the wave enters an attenuated regime with a complex $k_x = \pi/p - j\alpha$, where α is an attenuation constant. On the contrary, the glide-symmetry waveguide has always $-1 < A < 1$ in the neighborhood of zeros ($k_x = \pi/p$). Therefore, no stop-band is created at the Brillouin-zone edge due to the symmetry of this geometrical configuration, as explained in Section V.

VII. Conclusion

In this paper, we have discussed a novel method for accurately modeling corrugated surfaces embedded in a PPW environment. A homogenized model is not inaccurate for modeling moderately small values of the PPW thickness. This method was enhanced with the inclusion of higher-order harmonics to cover a wider range of thicknesses. Furthermore, a longitudinal circuit, whose parameters are known in close-form from rigorous mode-matching analysis, has been proposed based on T-junction models. This latter method shows close agreement with numerical full-wave simulations, even for extremely small values of thicknesses. It shows promise for the design of corrugated devices in gap waveguides [4] and artificial lenses [6]. Finally, the longitudinal circuit model can accurately model and explain a glide symmetry-corrugated waveguide. Glide symmetry has recently attracted strong interest due to its ultra-wideband response [13] and bandgap properties [15]. Extensive numerical results have fully validated the theoretical analysis.

References

[1] S. Maci, G. Minatti, M. Casaletti, and M. Bosiljevac, "Metasurfing: Addressing waves on impenetrable metasurfaces," *IEEE Antennas and Wireless Propagation Letters*, vol. 10, pp. 1499–1502, 2011.

[2] P. S. Kildal, "Artificially soft and hard surfaces in electromagnetics," *IEEE Transactions on Antennas and Propagation*, vol. 38, no. 10, pp. 1537–1544, Oct. 1990.

[3] P. S. Kildal, E. Alfonso, A. Valero-Nogueira, and E. Rajo-Iglesias, "Local metamaterial-based waveguides in gaps between parallel metal plates," *IEEE Antennas and Wireless Propagation Letters*, vol. 8, pp. 84–87, 2009.

[4] P.-S. Kildal, A. Zaman, E. Rajo-Iglesias, E. Alfonso, and A. Valero-Nogueira, "Design and experimental verification of ridge gap waveguide in bed of nails for parallel-plate mode suppression," *IET Microwaves, Antennas Propagation*, vol. 5, no. 3, pp. 262–270, Feb. 2011.

[5] M. Vukomanovic, J. L. Vazquez-Roy, O. Quevedo-Teruel, E. Rajo-Iglesias, and Z. Sipus, "Gap waveguide leaky-wave antenna," *IEEE Transactions on Antennas and Propagation*, vol. 64, no. 5, pp. 2055–2060, May 2016.

[6] C. Pfeiffer and A. Grbic, "A printed, broadband Luneburg lens antenna," *IEEE Transactions on Antennas and Propagation*, vol. 58, no. 9, pp. 3055–3059, Sep. 2010.

[7] M. Bosiljevac, M. Casaletti, F. Caminita, Z. Sipus, and S. Maci, "Non-uniform metasurface Luneburg lens antenna design," *IEEE Transactions on Antennas and Propagation*, vol. 60, no. 9, pp. 4065–4073, Sep. 2012.

[8] B. B. Tierney and A. Grbic, "A compact metamaterial beamformer designed through optimization," in *Proceedings of the IEEE International Symposium on Antennas and Propagation*, Jun. 2016, pp. 1–2.

[9] H. Bayer, A. Krauss, T. Zaiczek, R. Stephan, O. Enge-Rosenblatt, and M. A. Hein, "Ka-band user terminal antennas for satellite communications [antenna applications corner]," *IEEE Antennas and Propagation Magazine*, vol. 58, no. 1, pp. 76–88, Feb. 2016.

[10] C. Walter, "Surface-wave Luneberg lens antennas," *IRE Transactions on Antennas and Propagation*, vol. 8, no. 5, pp. 508–515, Sep. 1960.

[11] M. Casaletti, F. Caminita, and S. Maci, "Lens effect in parallel plate waveguide realized by using a metamaterial surface," in *Proceedings of the Fourth European Conference on Antennas and Propagation*, Apr. 2010, pp. 1–3.

[12] C. D. Diallo, O. Quevedo-Teruel, G. Valerio, H. Legay, and R. Sauleau, "Parallel-plate-waveguide Luneburg lens through a holey plate metasurface," in *2015 9th European Conference on Antennas and Propagation (EuCAP)*, May 2015, pp. 1–2.

[13] O. Quevedo-Teruel, M. Ebrahimpouri, and M. N. M. Kehn, "Ultrawideband metasurface lenses based on off-shifted opposite layers," *IEEE Antennas and Wireless Propagation Letters*, vol. 15, pp. 484–487, Dec. 2016.

[14] A. Hessel, M. H. Chen, R. C. M. Li, and A. A. Oliner, "Propagation in periodically loaded waveguides with higher symmetries," *Proceedings of the IEEE*, vol. 61, no. 2, pp. 183–195, Feb. 1973.

[15] M. Ebrahimpouri, E. Rajo-Iglesias, Z. Sipus, and O. Quevedo-Teruel, "Low-cost metasurface using glide symmetry for integrated waveguides," in *Proc. European Conf. Antennas Propag. (EuCAP)*, Apr. 2016.

[16] M. Bosiljevac, Z. Sipus, and P. S. Kildal, "Construction of Green's functions of parallel plates with periodic texture with application to gap waveguides - a plane-wave spectral-domain approach," *IET Microwaves, Antennas Propagation*, vol. 4, no. 11, pp. 1799–1810, Nov. 2010.

[17] G. Valerio, D. R. Wilton, D. R. Jackson, and A. Galli, "Acceleration of mixed potentials from vertical currents in layered media for 2-D structures with 1-D periodicity," *IEEE Transactions on Antennas and Propagation*, vol. 60, no. 8, pp. 3782–3793, Aug. 2012.

[18] N. Marcuvitz, *Waveguide Handbook*. Isha Books, 2013.

[19] R. Rodríguez-Berral, F. Mesa, and D. R. Jackson, "Gap discontinuity in microstrip lines: An accurate semianalytical formulation," *IEEE Transactions on Microwave Theory and Techniques*, vol. 59, no. 6, pp. 1441–1453, June 2011.

[20] Z. Sipus, H. Merkel, and P. S. Kildal, "Green's functions for planar soft and hard surfaces derived by asymptotic boundary conditions," *IEE Proceedings - Microwaves, Antennas and Propagation*, vol. 144, no. 5, pp. 321–328, Oct. 1997.

[21] C. Molero, R. Rodríguez-Berral, F. Mesa, and F. Medina, "Analytical circuit model for 1-D periodic T-shaped corrugated surfaces," *IEEE Transactions on Antennas and Propagation*, vol. 62, no. 2, pp. 794–803, February 2014.

[22] D. M. Pozar, "Microwave Engineering." John Wiley and Sons, Inc., 2011, ch. 8: Microwave Filters.

[23] G. Valerio, S. Paulotto, P. Baccarelli, P. Burghignoli, and A. Galli, "Accurate Bloch analysis of 1-D periodic lines through the simulation of truncated structures," *IEEE Transactions on Antennas and Propagation*, vol. 59, no. 6, pp. 2188–2195, Jun. 2011.

[24] A. Grbic and G. V. Eleftheriades, "Periodic analysis of a 2-D negative refractive index transmission line structure," *IEEE Transactions on Antennas and Propagation*, vol. 51, no. 10, pp. 2604–2611, Oct. 2003.

[25] P. Lampariello and A. A. Oliner, "New equivalent networks with simple closed-form expressions for open and slit-coupled E-plane Tee junctions," *IEEE Transactions on Microwave Theory and Techniques*, vol. 41, no. 5, pp. 839–847, May 1993.

[26] R. Quesada, D. Martín-Cano, F. J. García-Vidal, and J. Bravo-Abad, "Deep-subwavelength negative-index waveguiding enabled by coupled conformal surface plasmons," *Opt. Lett.*, vol. 39, no. 10, pp. 2990–2993, May 2014.

[27] J. J. Wu, C.-J. Wu, D. J. Hou, K. Liu, and T.-J. Yang, "Propagation of low-frequency spoof surface plasmon polaritons in a bilateral cross-metal diaphragm channel waveguide in the absence of bandgap," *IEEE Photonics Journal*, vol. 7, no. 1, pp. 1–8, Feb. 2015.

[28] M. Guglielmi and D. R. Jackson, "Broadside radiation from periodic leaky-wave antennas," *IEEE Transactions on Antennas and Propagation*, vol. 41, no. 1, pp. 31–37, Jan 1993.

[29] S. Paulotto, P. Baccarelli, F. Frezza, and D. R. Jackson, "Full-wave modal dispersion analysis and broadside optimization for a class of microstrip CRLH leaky-wave antennas," *IEEE Transactions on Microwave Theory and Techniques*, vol. 56, no. 12, pp. 2826–2837, Dec 2008.

[30] G. V. Eleftheriades and K. G. Balmain, *Negative-Refraction Metamaterials: Fundamental Principles and Applications*. Wileyy-IEEE Press, 2005.

[31] "CST Microwave Studio," http://www.cst.com/, version: 2016.